Electronic Supplementary Material (ESI) for Dalton Trans.

Probing the need of a very low axial zero field splitting in Mn^{II} systems with slow relaxation of the magnetization.

Evangelos Pilichos[a,b], Júlia Mayans[a] and Albert Escuer*[a]

[a] *Departament de Química Inorgànica i Orgànica, Secció Inorgànica and Institute of Nanoscience and Nanotecnology (IN²UB), Universitat de Barcelona, Marti i Franques 1-11, Barcelona-08028, Spain.*

[b] *Current address: Chemistry Departament, University of Cyprus, Nicosia-1678, Cyprus.*

*Albert Escuer, Email: albert.escuer@qi.ub.edu

Table S1. Crystal data and refinement details for complexes $\mathbf{1}_{NCS}$, $\mathbf{2}_{Cl}$ and $\mathbf{4}_{I}$.

	$\mathbf{1}_{NCS}$	$\mathbf{2}_{Cl}$	$\mathbf{4}_{I}$
Formula	$C_{57}H_{52}Mn_2N_{12}OS_4$	$C_{55}H_{60}Cl_4Mn_2N_8O_3$	$C_{105}H_{100}I_8Mn_4N_{16}O$
FW	1159.22	1132.79	2836.96
System	Triclinic	Monoclinic	Monoclinic
Space group	P1	$P2_1$	C2
a/Å	8.5398(4)	16.7866(10)	18.5020(11)
b/Å	10.3318(6)	8.6559(4)	9.0264(5)
c/Å	15.7479(9)	17.8003(11)	30.8068(18)
α/deg.	86.416(2)	90	90
ß/deg.	82.774(2)	98.624(2)	93.298(2)
γ/deg.	75.071(2)	90	90
V/ Å^3	1331.24(13)	2557.2(2)	5136.4(5)
Z	1	2	2
T, K	100(2)	100(2)	100(2)
Θ range/deg.	2.041-30.563	1.452-30.559°	1.986-30.596°
Reflex. collected	74662	53884	15581
Reflex. indep.	16202	15576	15581
Parameters	687	652	617
λ(MoKα), Å	0.71073	0.71073	0.71073
ρ_{calc}, g·cm^{-3}	1.446	1.471	1.834
μ(MoKα), mm^{-1}	0.685	0.757	2.941
Flack param.	0.04(3)	0.008(5)	0.05(2)
R	0.0595	0.0417	0.0360
ωR^2	0.0769	0.0978	0.0625

Table S2. Crystal data and refinement details for complexes **5_{Cl}**, **6_{Br}** and **7.**

	5_{Cl}	**6_{Br}**	**7**
Formula	$C_{14}H_{17}Cl_2MnN_3$	$C_{14}H_{17}Br_2MnN_3$	$C_{14}H_{17}MnN_9$
FW	353.14	442.06	366.30
System	Triclinic	Triclinic	Monoclinic
Space group	P-1	P-1	P 21/c
a/Å	7.4659(4)	7.4816(7)	15.505(1)
b/Å	7.8870(4)	8.1505(7)	8.2247(7)
c/Å	13.2290(7)	13.371(1)	12.859 (1)
α/deg.	76.203(2)	73.602(3)	90
ß/deg.	82.975(2)	85.395(3)	95.122(3)
γ/deg.	83.785(2)	83.015(3)	90
V/ Å^3	748.28(7)	775.5(1)	1633.3(2)
Z	2	2	4
T, K	100(2)	100(2)	100(2)
Θ range/deg.	3.678-30.610	2.746-30.617	2.943-30.531
Reflex. collected	24825	22456	37274
Reflex. indep.	4323	4618	4963
Parameters	183	183	248
λ(MoKα), Å	0.71073	0.71073	0.71073
ρ_{calc}, g·cm^{-3}	1.567	1.893	1.490
μ(MoKα), mm^{-1}	1.231	5.996	0.825
R	0.0191	0.0166	0.0330
ωR^2	0.0516	0.0406	0.0742

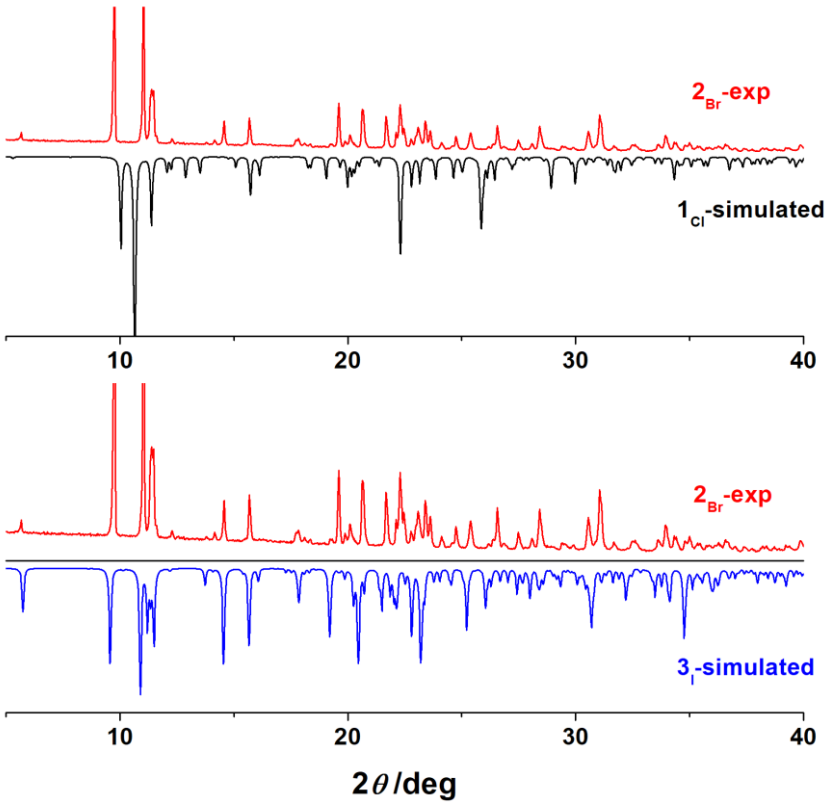

Fig. S1. Comparison of the PDXR spectra of complex $\mathbf{3}_{Br}$ with the simulated spectra of $\mathbf{2}_{Cl}$ and $\mathbf{4}_{I}$. The match with $\mathbf{4}_{I}$, with the consequent presence of two non equivalent *L* and *D* molecules in the cell agree with the EPR data.

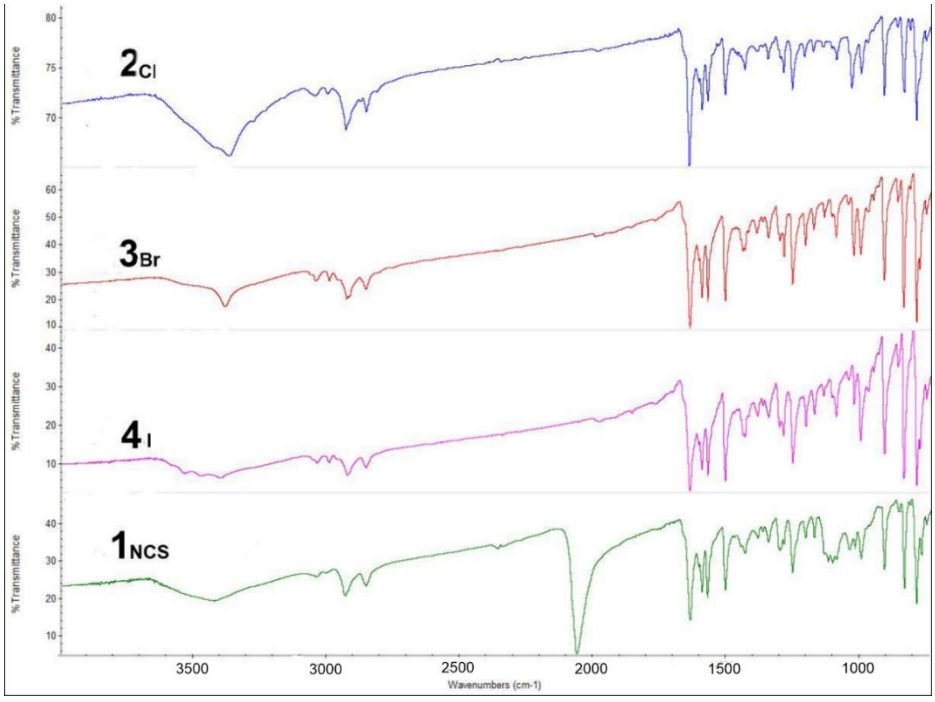

Fig. S2. IR spectra for complexes $\mathbf{1}_{NCS}$, $\mathbf{2}_{Cl}$, $\mathbf{3}_{Br}$ and $\mathbf{4}_{I}$. In agreement with the structural information the IR spectra are identical for the four complexes with the difference of the extra band corresponding to the stretching of the CN triple bond at 2066 cm^{-1} for $\mathbf{1}_{NCS}$.

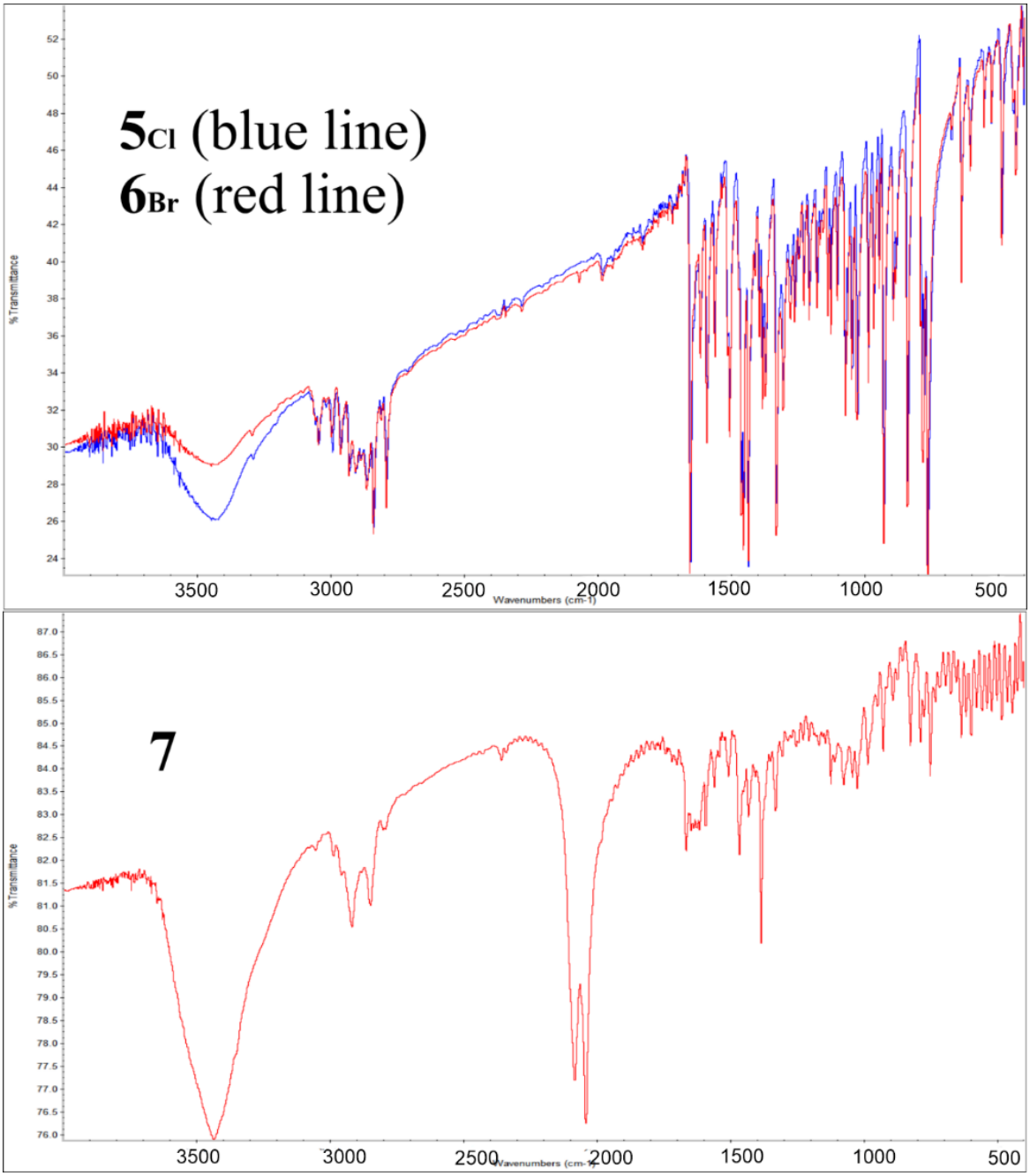

Fig. S3. IR spectra for complexes $\mathbf{5}_{Cl}$, $\mathbf{6}_{Br}$ and **7**. The spectra of the isostructural complexes $\mathbf{5}_{Cl}$, and $\mathbf{6}_{Br}$ are practically superimposables. The spectrum of complex **7** shows thw well differentiate bridging and terminal azido ligands.

Table S3. BSV values for the manganese cation for complexes $\mathbf{1}_{NCS}$, $\mathbf{2}_{Cl}$, $\mathbf{4}_{I}$, $\mathbf{5}_{Cl}$, $\mathbf{6}_{Br}$ and **7**.

	$\mathbf{1}_{NSC}$	$\mathbf{2}_{Cl}$	$\mathbf{4}_{I}$	$\mathbf{5}_{Cl}$	$\mathbf{6}_{Br}$	**7**
Mn^{II}	**2.175**	2.067	2.010	2.018	2.023	**2.075**

Table S4. SHAPE measures for the Mn^{II} cation of complexes $\mathbf{1}_{NCS}$, $\mathbf{2}_{Cl}$, $\mathbf{4}_{I}$, $\mathbf{5}_{Cl}$, $\mathbf{6}_{Br}$ and **7**. *S*(*P*) = 0 corresponds to a structure fully coincident in shape with the reference polyhedron P, regardless of size and orientation. The closest polyhedron is highlighted in red.

	$\mathbf{1}_{NSC}$	$\mathbf{2}_{Cl}$	$\mathbf{4}_{I}$	$\mathbf{5}_{Cl}$	$\mathbf{6}_{Br}$	**7**
***S*(HP-6)**	32.40	32.40	32.98	---	---	31.90
***S*(PPY-6)**	16.79	20.48	22.71	---	---	22.59
***S*(OC-6)**	**4.32**	**3.48**	**4.72**	---	---	**2.41**
***S*(TPR-6)**	6.98	9.10	9.89	---	---	10.77
***S*(JPPY-6)**	20.40	24.98	26.66	---	---	26.60
***S*(PP-5)**	---	---	---	30.22	30.65	---
***S*(vOC-5)**	---	---	---	7.66	8.11	---
***S*(TBPY-5)**	---	---	---	**3.42**	**3.60**	---
***S*(SPY-5)**	---	---	---	4.25	4.41	---
***S*(JTBPY-5)**	---	---	---	6.70	7.50	---

Ideal ML_6 polyhedra: HP-6 (D6h) Hexagon; PPY-6 (C5v) Pentagonal pyramid; OC-6 (Oh) Octahedron; TPR-6 (D3h) Trigonal prism; JPPY-6 (C5v) Johnson pentagonal pyramid J2

Ideal ML5 polyhedra: PP-5 (D5h) Pentagon; vOC-5 (C4v) Vacant octahedron; TBPY-5 (D3h) Trigonal bipyramid; SPY-5 (C4v) Spherical square pyramid; JTBPY-5 (D3h) Johnson trigonal bipyramid J12.

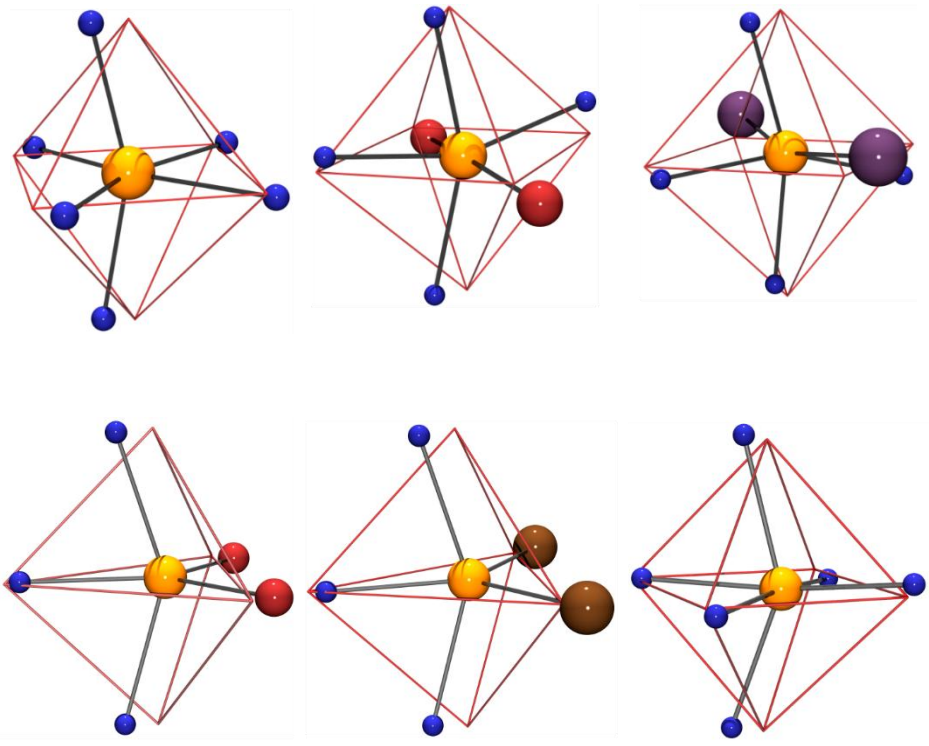

Fig. S4. Coordination environment and closest polyhedra for $\mathbf{1}_{NCS}$, $\mathbf{2}_{Cl}$, $\mathbf{4}_{I}$ **and**, $\mathbf{5}_{Cl}$, $\mathbf{6}_{Br}$ and **7**.

Table S5. Selected bond distances (Å) and angles (deg.) for complexes $\mathbf{1}_{NCS}$ (left) and $\mathbf{2}_{Cl}$ (right).

	$\mathbf{1}_{NCS}$ -*L*	$\mathbf{1}_{NCS}$ -*D*
Mn-N1	2.295(6)	2.268(6)
Mn-N2	2.236(5)	2.216(6)
Mn-N3	2.204(5)	2.207(5)
Mn-N4	2.298(6)	2.292(6)
Mn-N5	2.171(6)	2.189(6)
Mn-N6	2.166(6)	2.196(8)
N1-Mn-N2	81.7(2)	83.3(2)
N2-Mn-N3	75.6(2)	76.0(2)
N3-Mn-N4	82.3(2)	83.5(2)
N1-Mn-N4	120.5(2)	121.4(2)
N1-Mn-N3	157.2(2)	151.6(2)
N2-Mn-N4	157.6(2)	153.2(2)
N5-Mn-N6	156.7(2)	155.2(3)
N1-N2-N3-N4	4.9(3)	28.1(3)

	$\mathbf{2}_{Cl}$-A	$\mathbf{2}_{Cl}$-B
Mn-N1	2.275(3)	2.290(3)
Mn-N2	2.224(3)	2.232(3)
Mn-N3	2.207(3)	2.220(3)
Mn-N4	2.265(3)	2.316(3)
Mn-Cl1	2.569(1)	2.5241(9)
Mn-Cl2	2.496(1)	2.4658(9)
N1-Mn-N2	83.1(1)	82.78(10)
N2-Mn-N3	75.8(1)	75.49(10)
N3-Mn-N4	82.3(1)	81.46(10)
N1-Mn-N4	118.7(1)	120.03(11)
N1-Mn-N3	158.9(1)	158.01(10)
N2-Mn-N4	157.8(1)	156.82(10)
Cl1-Mn-Cl2	163.34(4)	164.67(3)
N1-N2-N3-N4	2.4(1)	0.7(1)

Table S6. Selected bond distances (Å) and angles (deg.) for complexes $\mathbf{4}_{I}$ (left), $\mathbf{5}_{Cl}$, $\mathbf{6}_{Br}$ (middle) and **7** (right).

	$\mathbf{4}_{I}$-*D*	$\mathbf{4}_{I}$-*L*
Mn-N1	2.293(7)	2.255(6)
Mn-N2	2.215(6)	2.234(6)
Mn-N3	2.212(7)	2.208(7)
Mn-N4	2.268(7)	2.281(6)
Mn-I1	2.949(1)	2.924(1)
Mn-I2	2.935(1)	2.888(1)
N1-Mn-N2	84.1(2)	82.4(2)
N2-Mn-N3	76.4(2)	76.3(2)
N3-Mn-N4	84.7(2)	82.1(2)
N1-Mn-N4	117.6(2)	119.1(2)
N1-Mn-N3	155.5(2)	158.7(2)
N2-Mn-N4	156.1(2)	158.4(2)
I1-Mn-I2	161.50(5)	163.13(5)
N1-N2-N3-N4	2.4(1)	0.7(1)

	$\mathbf{5}_{Cl}$	$\mathbf{6}_{Br}$
Mn-N1	2.3352(8)	2.329(1)
Mn-N2	2.1960(8)	2.186(1)
Mn-N3	2.3490(8)	2.353(1)
Mn-X1	2.3460(3)	2.4891(3)
Mn-X2	2.3648(3)	2.5094(3)
N1-Mn-N2	71.79(3)	72.18(4)
N2-Mn-N3	73.83(3)	73.91(4)
N1-Mn-X1	105.11(2)	105.65(3)
N2-Mn-X1	127.25(2)	126.67(3)
N3-Mn-X1	100.53(2)	100.20(3)
N1-Mn-X2	117.6(2)	93.06(3)
N2-Mn-X2	121.18(2)	120.84(3)
N3-Mn-X2	96.91(2)	98.06(3)
X1-Mn-X2	111.57(1)	112.480(9)

	7
Mn-N1	2.331(1)
Mn-N2	2.218(1)
Mn-N3	2.365(1)
Mn-N4	2.184(1)
Mn-N6’	2.293(2)
Mn-N7	2.120(1)
N1-Mn-N2	72.18(5)
N2-Mn-N3	74.15(5)
Mn-N4-N5	143.9(1)
Mn-N6’-N5’	142.1(1)
Mn-N4···N6-Mn’	135.7(1)

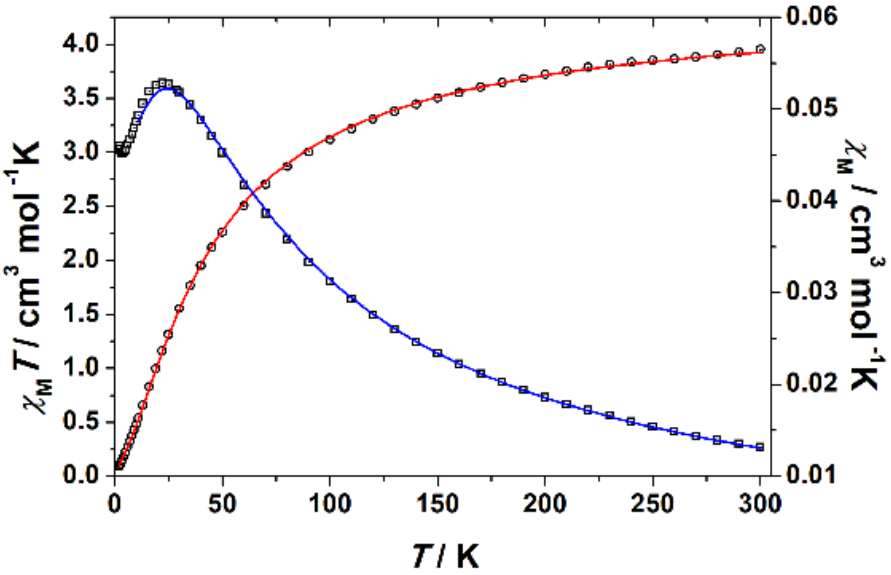

Fig. S5. $\chi_M T$ (left axis) and χ_M (rigth axis) vs. temperature for complex **7**. Solid lines ($\chi_M T$, red, χ_M blue) show the best fit of the experimental data

The room temperature $\chi_M T$ value is 3.96 $cm^3 \cdot mo^{l-1} \cdot K$, slightly lower than the expected value of 4.375 $cm^3 \cdot mo^{l-1} \cdot K$ for one isolated S = 5/2 paramagnetic center. On cooling the $\chi_M T$ value decreases continuously, tending to zero at low temperature. In agreement with this antiferromagnetic response the χ_M plot exhibits a maximum of susceptibility at 22 K. Fit of the experimental data applying the Hamiltonian $H = -J\Sigma(S_i * S_{i+1})$ yields the best fit parameters J = 2.01(1) cm^{-1} and g = 2.005(1).

The magnetic response mediated by an end-to-end azido bridge between two Mn^{II} cations gives the maximum antiferromagnetic response for a planar Mn-NNN-Mn arrangement (torsion 180º) and a Mn-N-N bond angle of 110º.[35] Larger bond or lower dihedral angles can reduce but not suppress the antiferromagnetic interaction and the sign and magnitude of the calculated coupling constant agree with the expected value for a single end-to-end azido bridge with moderately large bond angles.[36]

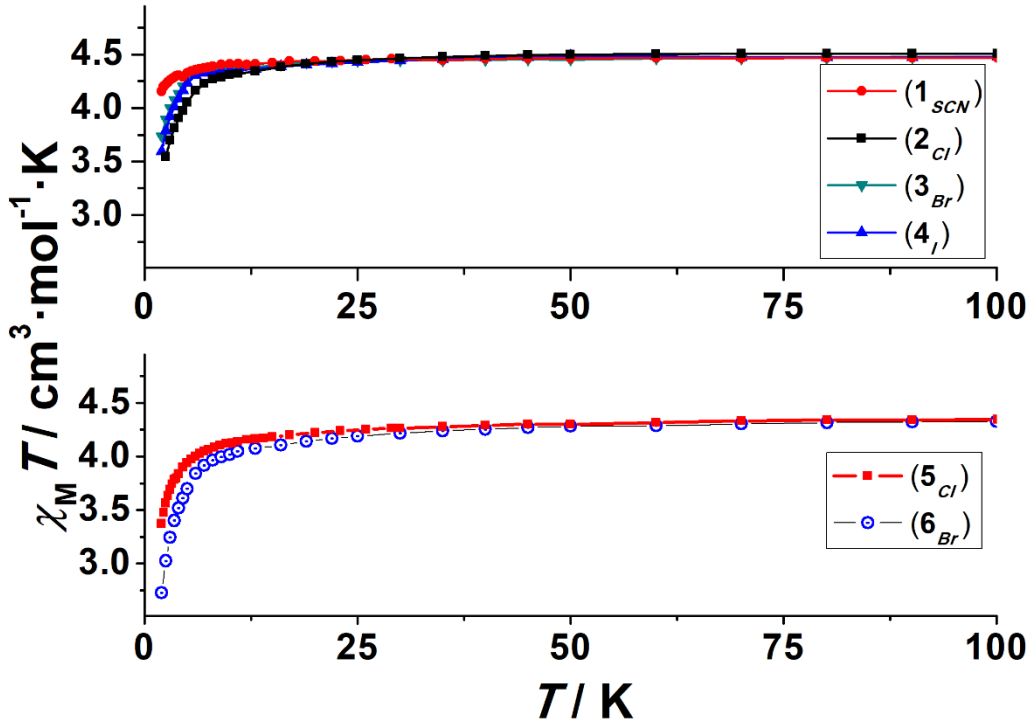

Fig. S6. $\chi_M T$ vs. temperature plots for complexes $\mathbf{1}_{NCS}$, $\mathbf{2}_{Cl}$, $\mathbf{3}_{Br}$, $\mathbf{4}_{I}$ (top) $\mathbf{5}_{Cl}$ and $\mathbf{6}_{Br}$ (bottom).

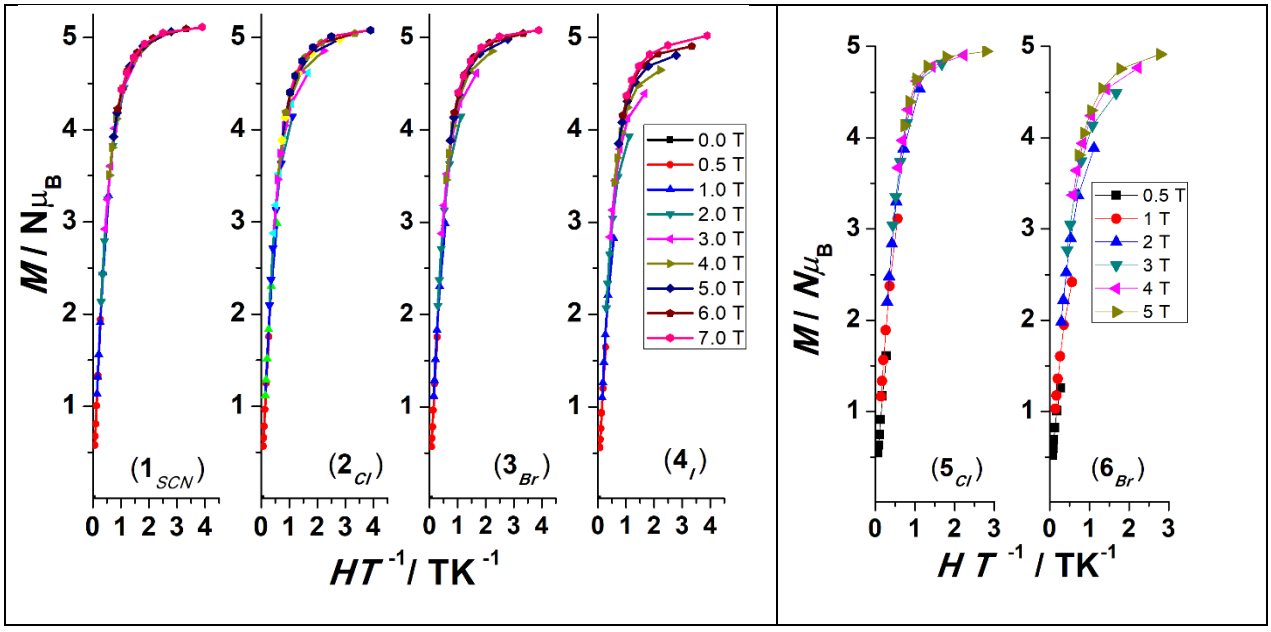

Fig. S7. Reduced magnetization plots for complexes $\mathbf{1}_{NCS}$, $\mathbf{2}_{Cl}$, $\mathbf{3}_{Br}$, $\mathbf{4}_{I}$, $\mathbf{5}_{Cl}$ and $\mathbf{6}_{Br}$.

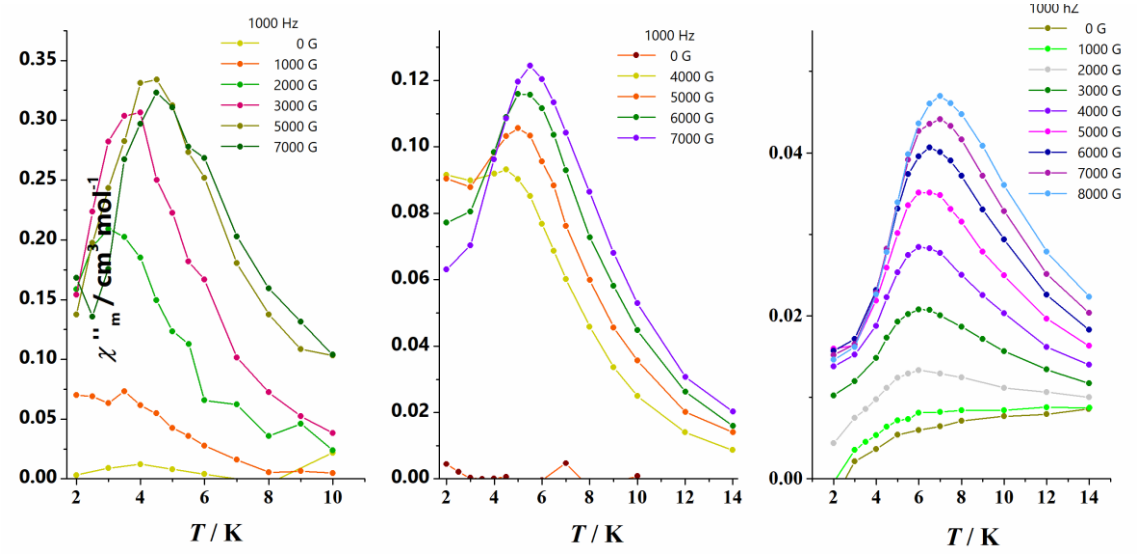

Fig. S8. Field dependence of χ''_M *vs*. (*T*,*H*) for complexes $\mathbf{1}_{NCS}$, $\mathbf{2}_{Cl}$ and $\mathbf{5}_{Cl}$.

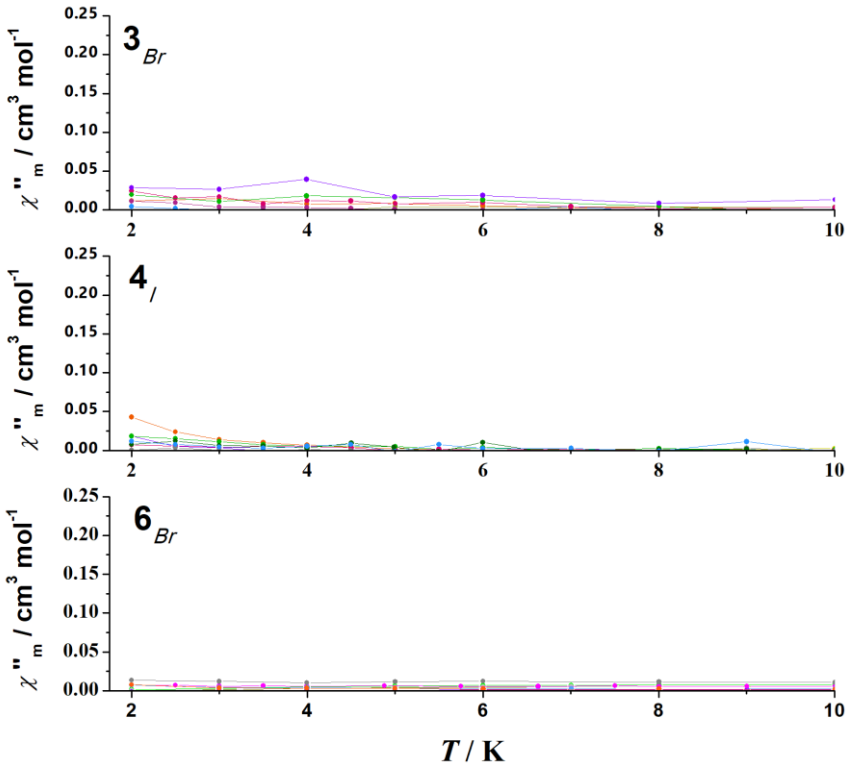

Fig. S9. From top to bottom, field dependence of χ''_M *vs*. (*T*,*H*) for complexes $\mathbf{3}_{Br}$, $\mathbf{4}_{I}$ and $\mathbf{6}_{Br}$ measured in the 0-1 T range.

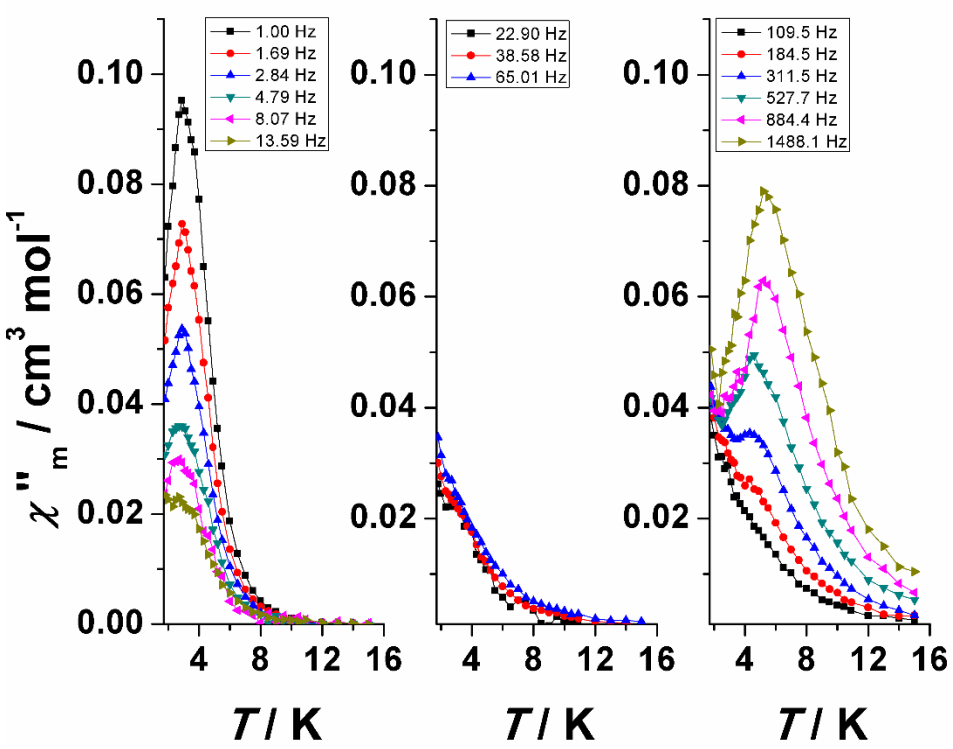

Fig. S10. Detail of the χ'_M *vs*. *T* response of complex **2**$_{Cl}$ for low, intermediate and large frequencies, showing the high and low frequency well isolated relaxation processes.

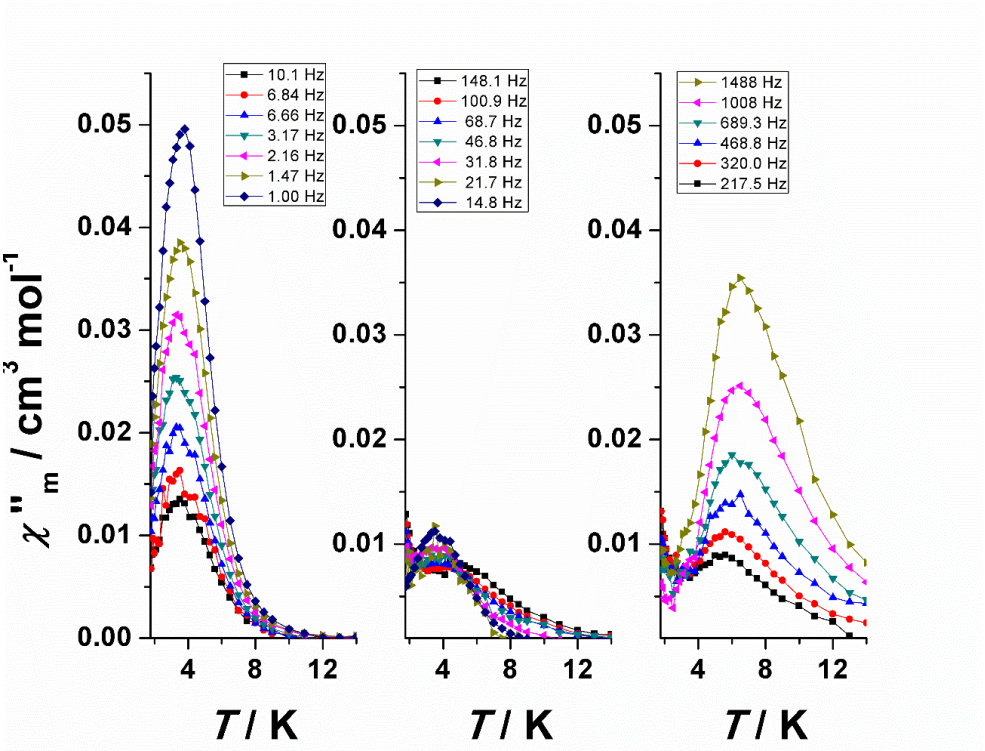

Fig. S11. Detail of the χ'_M *vs*. *T* response of complex **5**$_{Cl}$ for low, intermediate and large frequencies, showing the high and low frequency well isolated relaxation processes.

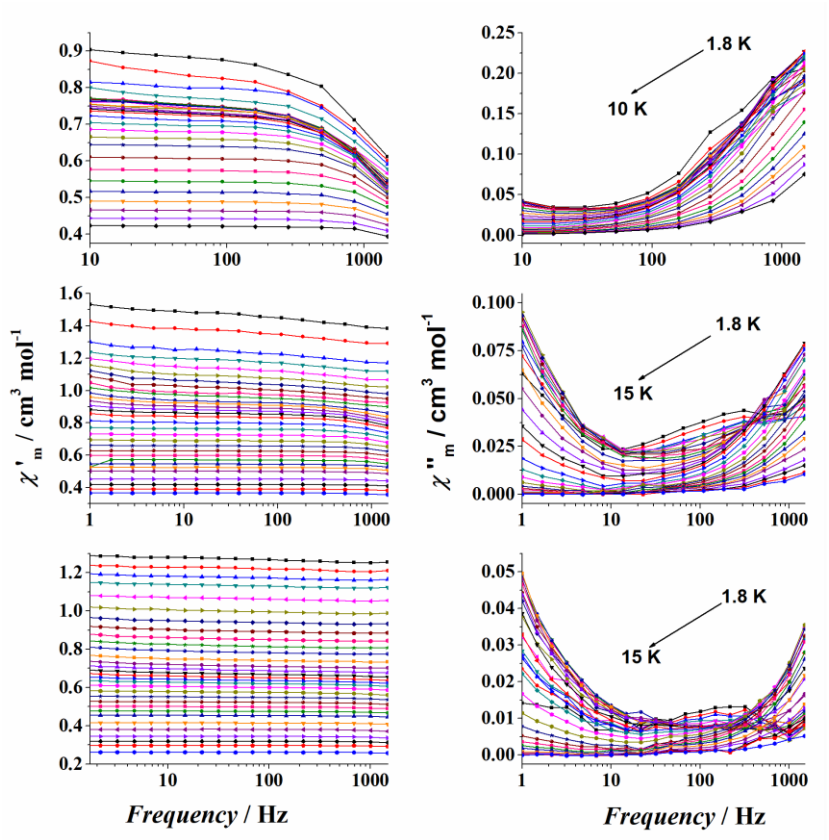

Fig. S12. Plot of χ'_M (left) and χ''_M (right) *vs*. frequency for complexes $\mathbf{1}_{NCS}$, $\mathbf{2}_{Cl}$, and $\mathbf{5}_{Cl}$.

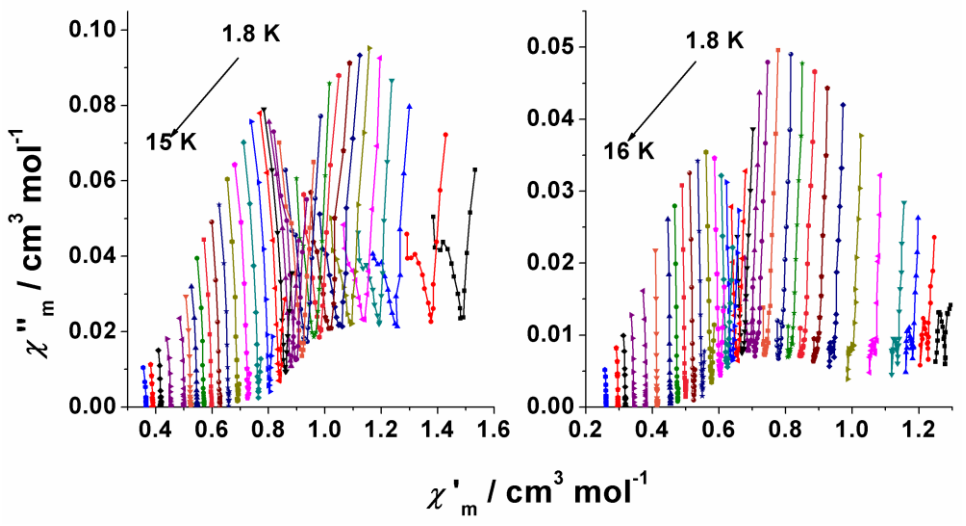

Fig. S13. Argand plot for complexes $\mathbf{2}_{Cl}$ and $\mathbf{5}_{Cl}$. The very partial semicircles excluded to extract relaxation data for these two compounds.

Table S7. Tau values and residual from the fit of the Argand plot of complex $\mathbf{1}_{NCS}$.

T	dChi	Tau	Alpha	Residual
4.10956	0.43738	9.30E-05	3.33E-07	1.31E-04
4.31162	0.43894	9.16E-05	4.35E-07	1.00E-04
4.49313	0.43898	8.70E-05	4.61E-07	5.14E-05
4.8004	0.44537	8.22E-05	5.49E-07	4.98E-05
5.10028	0.43785	7.81E-05	6.83E-07	4.98E-05
5.40033	0.42932	7.39E-05	8.01E-07	4.68E-05
5.70057	0.42584	6.89E-05	8.34E-07	1.48E-05
6.00004	0.39432	6.38E-05	1.06E-06	1.94E-05
6.50021	0.36637	5.82E-05	1.36E-06	7.72E-06
6.99994	0.35591	5.11E-05	1.87E-06	8.19E-06
7.5005	0.32553	4.92E-05	2.61E-06	7.93E-06
8.00059	0.30459	4.51E-05	2.96E-06	6.36E-06
8.00059	0.29196	4.13E-05	3.09E-06	1.41E-05
9.00098	0.2686	3.78E-05	4.37E-06	1.56E-05
9.50041	0.24149	3.63E-05	3.91E-06	3.07E-05

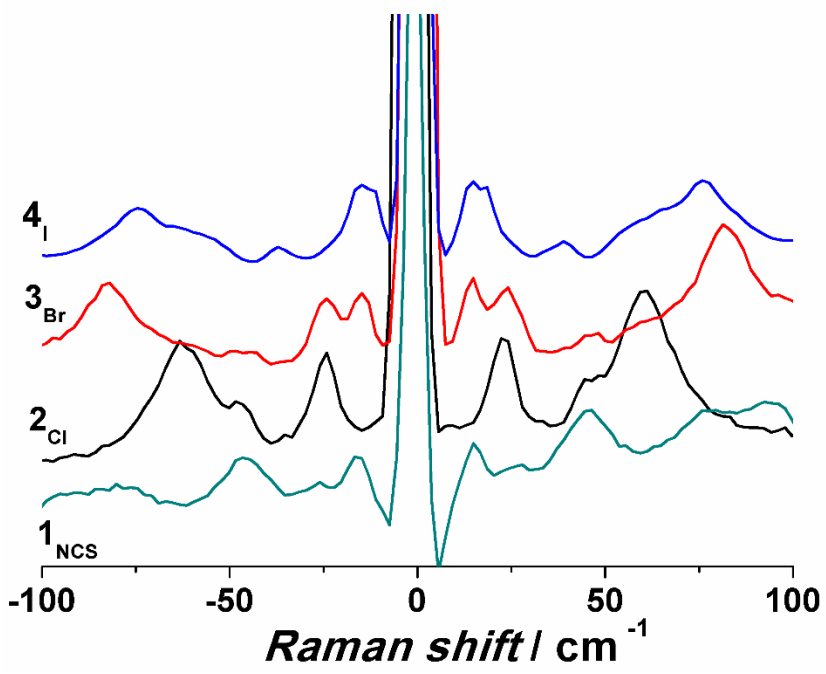

Fig. S14. Raman spectra in the Tz region for complexes $\mathbf{1}_{NCS}$, $\mathbf{2}_{Cl}$, $\mathbf{3}_{Br}$ and $\mathbf{4}_{I}$,.